FEM simulation of single beard hair cutting with foil–blade–shaving system

Article *in* Journal of the Mechanical Behavior of Biomedical Materials · March 2015

DOI: 10.1016/j.jmbbm.2015.03.002

2 authors, including:

Gang Fang
Tsinghua University
71 PUBLICATIONS **439** CITATIONS

SEE PROFILE

JOURNAL OF THE MECHANICAL BEHAVIOR OF BIOMEDICAL MATERIALS 46 (2015) 271–284

Available online at www.sciencedirect.com

ScienceDirect

www.elsevier.com/locate/jmbbm

Research Paper

FEM simulation of single beard hair cutting with foil–blade-shaving system

Gang Fang[a,b,*], Alois Köppl[c]

[a]Department of Mechanical Engineering, Tsinghua University, Beijing 100084, China
[b]State Key Laboratory of Tribology, Tsinghua University, Beijing 100084, China
[c]Braun GmbH, Frankfurter Str. 145, D-61476 Kronberg im Taunus, Germany

ARTICLE INFO

Article history:
Received 18 November 2014
Received in revised form
4 March 2015
Accepted 8 March 2015
Available online 14 March 2015

Keywords:
Cutting
Beard hair
Finite element method
Skin

ABSTRACT

The performance of dry-shavers depends on the interaction of the shaving components, hair and skin. Finite element models on the ABAQUS/Explicit platform are established to simulate the process of beard hair cutting. The skin is modelled as three-layer structure with a single cylindrical hair inserted into the skin. The material properties of skin are considered as Neo-Hookean hyper-elastic (epidermis) and Prony visco-elastic (dermis and hypodermis) with finite deformations. The hair is modelled as elastic–plastic material with shear damage. The cutting system is composed of a blade and a foil of shaver. The simulation results of cutting processes are analyzed, including the skin compression, hair bending, hair cutting and hair severance. Calculations of cutting loads, skin stress, and hair damage show the impact of clearance, skin bulge height, blade dimension and shape on cutting results. The details show the build-up of finite element models for hair cutting, and highlight the challenges arising during model construction and numerical simulation.

1. Introduction

Since the American inventor King Camp Gillette invented a safety shaver with disposable blades in 1904 (Gillette, 1904), there was a revolution in beard hair cutting. Hair cutting has become rapid, clear and safe. The shavers introduced by Gillette consist of one or more blades which are moved against beard hairs. Those hairs are supported by the surrounding skin and are cut provided the skin can withstand the force which is exerted from the blade onto the hair without too large deformations. This force is equal to the cutting force and depends on the hair properties and the blade design. Under dry conditions the cutting force is so high that skin deformations become too large. As consequence, blades engage hairs less effectively or hairs are uncomfortably pulled out of the skin. In the first case, the skin retracts together with the hair so that the hair vanishes within the skin rather than being cut. In the second case, hairs are pulled so far out of the skin that pain arises. That is the reason why the application of safety shavers requires a pre-treatment of the beard with shaving cream. The pre-treatment reduces the hair stiffness and thus the force necessary for optimal pulling and cutting. The requirement of this pre-treatment was the motivation for the introduction of electric shavers. They have rotating or oscillating cutting systems and

*Corresponding author. Tel: +86 10 62782694.
E-mail address: fangg@tsinghua.edu.cn (G. Fang).

http://dx.doi.org/10.1016/j.jmbbm.2015.03.002
1751-6161/

Nomenclature

C_{10}	a material constant of Neo-Hookean hyper-elasticity model
D_1	a material constant of Neo-Hookean hyper-elasticity model
λ_1, λ_2 and λ_3	the principal stretches
I_1	the first strain invariant, $I_1=\lambda_1^2+\lambda_2^2+\lambda_3^2$
J	the volume ratio, $J=\lambda_1\lambda_2\lambda_3$
T	time
$g(t)$	the dimensionless shear relaxation modulus
g_i, $_{i=1,2}$	material constants of the two-term Prony series of visco-elasticity
τ	material constants of the two-term Prony series of visco-elasticity
G	the instantaneous shear modulus

Fig. 1 – Typical dry shaver with cutting tools.

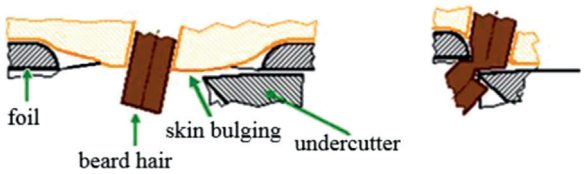

Fig. 2 – Schematic of a beard hair cutting through single foil aperture with skin bulging into aperture, and undercutter approaching and severing a hair.

can be applied to dry beard. A typical dry shaver with magnified cutting tools is shown in Fig. 1.

The schematic process of hair cutting within dry shavers is shown in Fig. 2. The main cutting tools include an under-cutter with a series of blades and a foil with apertures as the upper cutter. When the shaver and the foil are moved across the face, skin with hairs is compressed into foil apertures, and forms bulges. The under-cutter with its blades oscillates under the foil so that the blades approach hairs. The hair is bent and gets in contact with the foil edge. After undergoing elastic and plastic deformations, the hair is damaged to fracture between the blade and the foil edge.

Advantage of wet shaving is that the hair is pulled out of the skin before being cut, while the disadvantage is the necessity of the pre-treatment. Advantage of dry shaving is that there is no need for the pre-treatment while the disadvantage is that the beard cannot be cut so deeply as in case of wet shaving.

Blade design determines the shaver's efficiency and life-time. The investigation of the hair cutting process is necessary to understand the influence of the blade geometry and dimensions on the cutting results. Numerical simulation of cutting processes has become an effective tool for predicting cutting processes, especially for metallic materials. This suggests applying this method to hair cutting research. Challenges are the following:

(1) Material mechanical behaviour (stress–strain data, friction, and fracture);
(2) Rational models of hair and blade; and
(3) Modelling of hair cutting process.

The mechanical behaviour and structure of hair are complex. A hair consists of cuticle, cortex and medulla. Hair is thus a 'sandwich' material (Dawber, 1996). Thozhur et al. (2006) studied the three main morphological features of beard hair. In their investigation, a novel microscopy method was developed that enabled the cross-sectional area of beard hair to be determined by taking measurements at a few angles of rotation of the hair. The measurements revealed that a majority of the beard hair samples had an elliptical type cross-section. The investigation for the tensile stress–strain behaviour of human beard hair was also introduced. The experimental results showed that the general stress strain curve is similar to that observed in case of scalp hair with three distinct regions namely, elastic, yield and post yield region. The results from the tensile tests indicate that there is a strong effect of moisture on the Young's modulus and yield stress. Both are brought down nearly by a factor of 3.0. There appears to be some variation with facial site, subject and strain rate. Seshadri and Bhushan (2008) carried out in situ tensile loading experiments on hair with atomic force microscopy (AFM), and analyzed the response of human hair fibres, specifically the surface cuticular structure. They also got stress–strain curves for five types of hair: virgin, virgin treated, chemically damaged, chemically damaged treated and mechanically damaged. The stress data obtained in their tests are lower than those obtained by Thozhur et al. (2006), but the values of Young's module and fracture strain are close. Barnes and Roberts (2000) analyzed the non-linear viscoelastic behaviour of human hair. They succeeded to characterize it reasonably well by a mathematical expression containing simple and separate functions of time and extension. Bhushan (2005, 2008) focussed on the tribological characteristics of hair and skin.

Friction experiments were performed at a range of loads, speeds, and skin area in order to study their effect on skin–hair and hair–hair contacts. Conducted measurements revealed average coefficients of friction for different ethnicities and hair types (Wei and Bhushan, 2006). The coefficient of friction of Caucasian (unsoaked and soaked) and Asian (unsoaked) hair were measured and compared.

Literature on the numerical simulation of hair cutting is scarce to date. Experimental research on the other hand is available. Thozhur et al. (2007) studied cutting forces and cutting mechanisms of beard hair. High speed cutting tests on real beard hair samples showed the influence of variables such as subject age, moisture and sample ageing on the cutting properties. Sakon et al. (2009) investigated the cutting blade material and treatment. Focus is the effect of surface modification to the movable blade. It is fabricated from hardened SUS420J2Mo by applying iron nitriding, ion plating, and plasma CND processes, in order to improve the cutting performance and lifetime. The published research results above provided some hints for the numerical simulation of hair cutting and are taken as basis.

The present study comprises simulations of hair cutting processes based on finite element method (FEM) models. 2-D models are adopted to improve the calculation efficiency of the deformation and fracture of the hair. Even some boundary conditions have to be simplified, the simulations provide insightful understanding of beard hair cutting, including hair deformation and fracture, skin stress and strain, and show the effects of the cutting parameters and blade parameters on cutting results.

2. Material parameters of hair and skin

For getting reliable simulation results, realistic material parameters are necessary. In hair cutting simulation, the hair undergoes elastic deformation, plastic deformation and damage. The skin forms vital boundary conditions for hair deformation and cutting. Its properties are consequently needed for hair cutting.

2.1. Mechanical properties of hair

A schematic of the hair structure is shown in Fig. 3 and exhibits non-linear viscoelastic behavior. From surface to center of cross-section, a hair fiber consists of three layers, of the cuticle, the cortex and the medulla (van de Sompela et al., 2009). By SEM, the cuticle was found to consist of flat overlapping cells. Each cuticle cell is approximately 0.3–0.5 μm thick and 5–10 μm long. The cuticle of human hair has up to 5–10 cells through the thickness (Bhushan, 2008). Near the scalp the cells are well established, between scalp and the tips the cells appear worn and toward the tips the cells vanish more and more. The cortex contains cortical cells and intercellular binding material. The cells are generally 1–6 μm thick and 100 μm long (Bhushan, 2008). The medulla makes up a small percentage of the mass of the whole hair. It is believed (Bhushan, 2008) that the medulla has a negligible contribution to the mechanical properties of human hair fibers. The hardness and elastic modulus of hair surface decreases from root to tip (Bhushan, 2008). The cuticles contribute more to the hair lateral mechanical properties than the cortex, and the hardness of the cuticle is larger than that of cortex.

Stress data such as elastic–plastic constitutive relationships for pure cuticle, cortex or medulla are hardly available. The mechanical properties of hair vary with ethnicity (Asian, Caucasian and African), position (near scalp, middle and near tip), and environment conditions, in particularly with humidity. The present research is based on data from Thozhur et al. (2006), which was derived from the middle part of Caucasian hair. There are few public reports of hair anisotropic in mechanical properties. In present study, the hair is assumed as isotropic. Utilized data is shown in Fig. 4 and Table 1. Taking into account that the present research focuses on dry

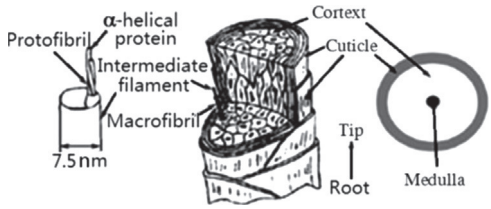

Fig. 3 – Structure of hair (Thozhur et al., 2006).

Table 1 – Plastic stress–strain data of the dry hair.

Plastic strain	0.0	0.05	0.10	0.15	0.25	0.27
Stress (MPa)	100	140	145	150	160	180

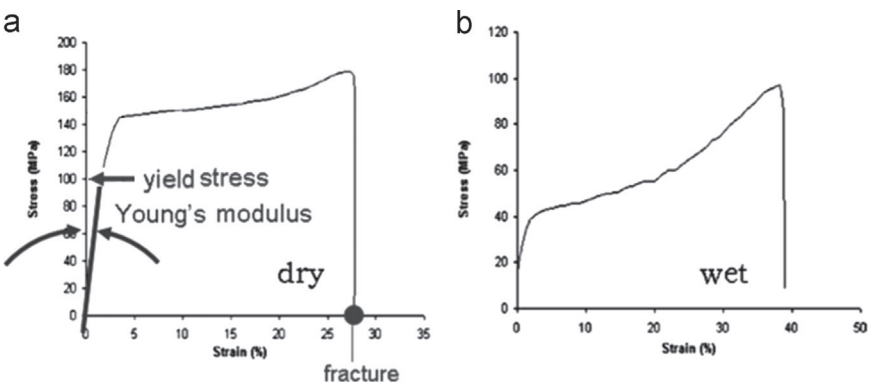

Fig. 4 – Tensile tests stress–strain curves of hair at (a) dry, (b) wet conditions (Thozhur et al., 2006).

cutting, an elastic modulus of 3.56 GPa is used (Thozhur et al., 2006). The value was derived through curve-fitting. Hair's Poisson ratio is 0.3 (Xu and Chen, 2011), and the density is 1200 kg/m^3. Constitutive dates are close to those used in other calculations (Xu and Chen, 2011), where the hair curling process was simulated by FEM and the residual stress/strain were focused on. Characteristic time of the visco-elasticity is of the magnitude of 10–100 s. Cutting time is of the magnitude of 0.001 s. Therefore, the hair's viscous-elastic characteristic is omitted.

The mentioned hair data were applied throughout the entire hair cross-section. That is, differences between the mechanical properties of hair layers were not taken into account. Reason is that no further data were available for the plastic behaviour of the three layers. Though Young's modules are available for the different layers, simulations with different magnitudes of elasticity indicated a small impact of Young's modulus on cutting force under large plastic deformation.

Hair fracture data is vital to cutting process simulation. Fracture is based on the shear damage model. It is introduced into the ABAQUS code by help of the shear damage initiation criterion which models the onset of damage due to shear band localization. Following this model damage starts at a critical value of equivalent plastic strain. The critical equivalent plastic strain is selected to be 0.27 according to the experimental data (Fig. 4). Thus, when the equivalent plastic strain within an element is reached, the element is removed.

2.2. Mechanical properties of skin

Skin has to be considered during hair cutting simulation since it determines boundary conditions of the hair deformation process. Skin stress is also an important index, because high skin stress leads to irritation or skin lesions. Draelos (2012) reviewed some issues related to the relationship between hair shaving technology and skin health.

Skin includes the three layers: epidermis, dermis and hypodermis. The epidermis including its top layer stratum corneum is typically described by a hyper-elastic constitutive model, and dermis and hypodermis by viscous-elastic constitutive models (Flynn and McCormack, 2008). Hyper-elastic models consider large strain deformations of skin, but neglect the material rate-dependence, stress relaxation and hysteretic behaviours. The available models are built on the definition of the strain energy function. The present simulations are performed with a hyper-elastic model for the epidermis using the Neo-Hookean hyper-elastic function. It has the strain energy potential

$$W = C_{10}(I_1 - 3) + \frac{1}{D_1}(J-1) \quad (1)$$

where C_{10} and D_1 are material constants, $J=\lambda_1\lambda_2\lambda_3$ is the volume ratio and $I_1 = \lambda_1^2 + \lambda_2^2 + \lambda_3^2$ is the first strain invariant defined through the principal stretches λ_1, λ_2 and λ_3.

Epidermis constitutive data are taken from research work of Flynn and McCormack (2008) at relative humidity of 75%, i.e. $C_{10}=40$ MPa and $D_1=0.00101$ MPa. Utilizing the ABAQUS curve fitting tool shows these values to be equivalent to an elastic modulus of 240 MPa. The density of the epidermis is 1100 kg/m^3 (Pailler-Mattei et al., 2008), and it includes the stratum corneum.

Table 2 – Viscoelastic parameter of Prony model of skin and subcutaneous (Wu et al., 2006).

	g_1	τ_1 (s)	g_2	τ_2(s)
Dermis	0.295	0.373	0.349	5.592
Hypodermis	0.090	0.294	0.215	9.557

For skin dermis and hypodermis, viscoelasticity was modelled using the QLV (Quasi Linear Viscoelasticity) approach with the reduced relaxation function represented by a Prony series. The present simulations adopt the viscoelastic data corresponding to Table 2 and the two-term Prony series:

$$g(t) = [1 - g_1(1 - e^{-t/\tau_1}) - g_2(1 - e^{-t/\tau_2})] \quad (2)$$

where t is time, $g(t)$ is the dimensionless shear relaxation modulus, and g_i and τ_i are material constants. The dimensionless modulus is defined as the ratio of the shear relaxation modulus and the instantaneous shear modulus G. The duration of cutting a hair is very short (less than 2.0 ms) relative to relaxation time list in Table 2. Therefore, the weak viscoelastic effects of skin layers of the dermis and the hypodermis in present model will be reflected. In the further simulation of multiple hair cutting or constitutive cutting with the blade oscillation, the viscoelasticity of skin will be more effective than the present model of single hair cutting.

Other parameters of dermis include the density of 1100 kg/m^3, the elastic modulus of 5 MPa, and the Poisson ratio of 0.4. The density of the hypodermis is equal to that of the dermis. The elastic modulus is 1 MPa and the Poisson ratio 0.4.

3. Modeling of hair cutting

3.1. Geometry model

ABAQUS/Explicit FEM program was selected to model the cutting process of hair. The skin structure is typically divided into three layers. From the outer to the inner, the first layer is the epidermis with its surface layer called stratum corneum, the middle layer is the dermis, and the bottom layer is the subcutaneous layer.

The thickness of human skin varies considerably with sex, race, body site and age. Delalleau et al. (2008) showed their research results of in vivo measurements for forearm skin thickness from 150 tests that were performed on 30 individuals. The minimal value found was 860 μm, the maximal one was equal to 1510 μm and the average was 1.080 mm. Pellacani and Seidenariv (1999) gave values for facial skin thickness based on a study on 40 healthy Caucasian women. The average value of skin thickness was 2.1 mm at chin, 2.5 mm at upper lip and 1.7 mm at cheek. In the present simulation, total thickness of skin in the present model of 1.54 mm is used.

The division of the skin into its sub-layers is based on published material data (Flynn and McCormack, 2008). Wiltton and Everal (1973) investigated the epidermis thickness at six main body sites. The average thickness of face skin epidermis

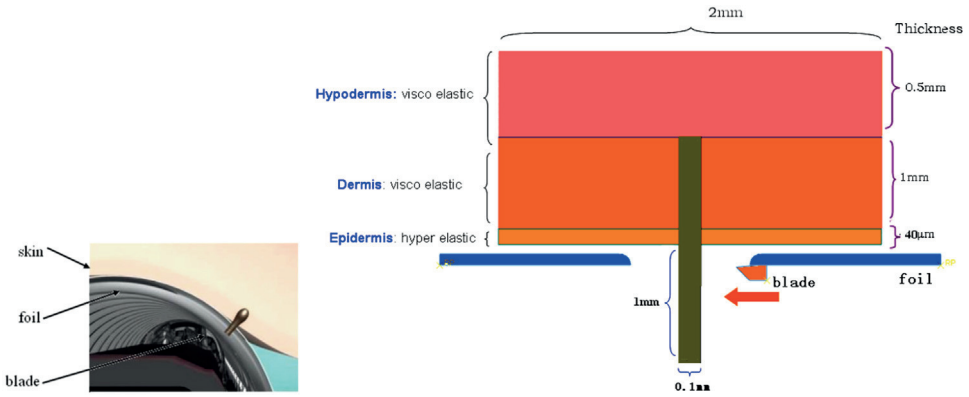

Fig. 5 – Whole geometry model of hair cutting.

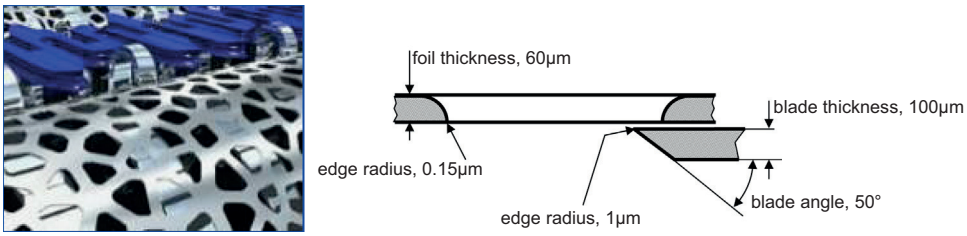

Fig. 6 – Geometry model of foil and blade.

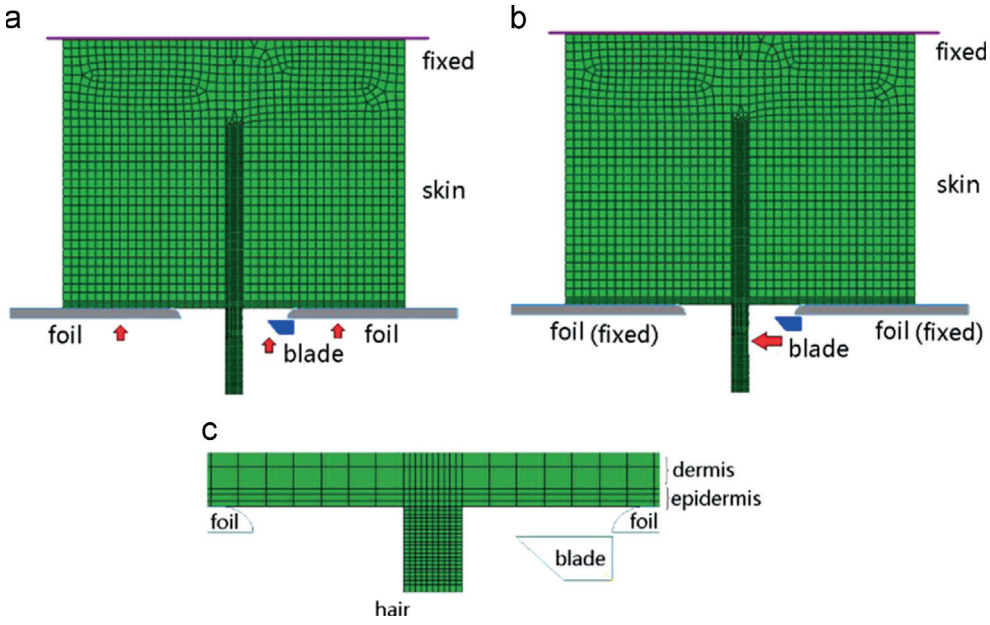

Fig. 7 – Two-dimensional (2D) finite element model of hair in skin and contact with foil (a) step1, compression, (b) step2 cutting, and (c) zoom in view of meshes near hair root.

was 49.8 μm, and 38.8 μm at cheek sites. Consequently, the epidermis in the present model is 40 μm.

For dermis thickness, we adopted 1.0 mm (Delalleau et al., 2008). Thus, the hypodermis thickness in the present model turns out to be 0.5 mm.

The geometry model for hair cutting is shown in Fig. 5. Hair is an outgrowth of filamentous cells, containing keratin, that grows from follicles found in the dermis. In the cutting model, the hair was inserted into epidermis and dermis, and the hypodermis was considered as soft base. Fig. 6 lists the dimensions of blade and foil. The foil aperture width is 0.6 mm, the thickness is 60 μm and edge radius is 0.15 μm. The blade has an edge radius of 1 μm, a wedge angle of 50 degree, and a thickness 0.1 mm. The clearance between the blade and the foil is 10 μm.

3.2. *FEM model*

The deformations of the foil and the blade are negligible compared to those of skin and hair. Foil and blade are consequently considered as rigid bodies, so that no meshes are

allocated. Foil and blade are considered only as boundaries. Skin and hair were discretized into quadrilateral elements. Alternative elements such as triangular ones would yield results with smaller accuracy. The expected fracture area within the hair was meshed by finer meshes than other areas, which was for the more accurate treatment of damage during cutting simulation. The mesh sizes of the hair, the epidermis and the dermis/hypodermis are 0.01 mm, 0.013 mm and 0.05 mm, respectively. Simulation results proved that these values got a good balance between efficiency and the precision of calculation.

Hair and skin are discretized via uniform meshes. The corresponding regions differ only by their material properties. The hair shares the interfaces nodes with the skin. In fact, the skin and the hair were segregated by some boundary lines, which were shared by the skin and the hair. The skin top side which corresponds to the inner surface of the hypodermis is fixed. The left and right sides of skin are considered to be free. Simulations with the other extreme of fixed boundaries will be

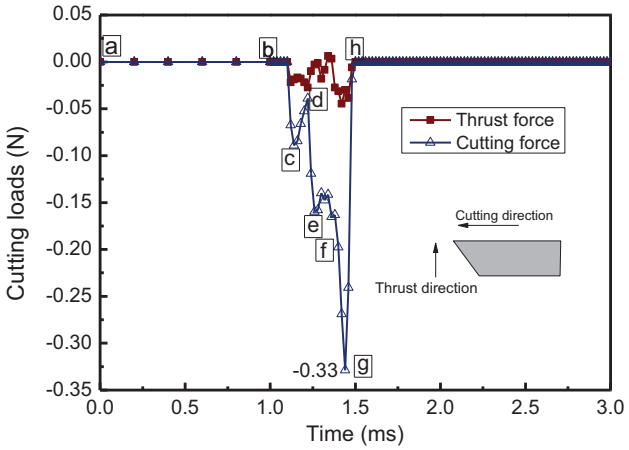

Fig. 9 – Blade cutting loads varying with the cutting process for hair with thickness of 0.1 mm based on the plane model.

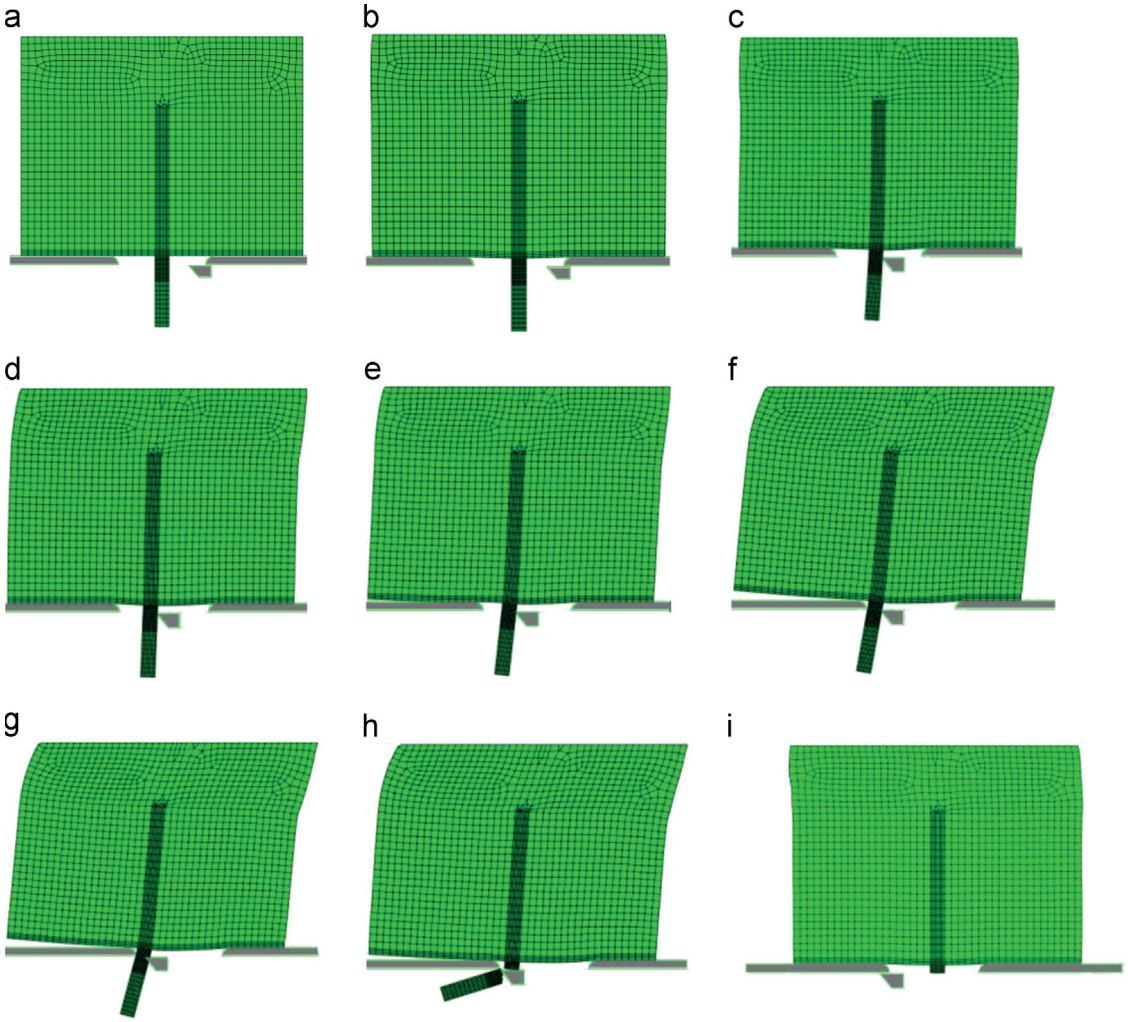

Fig. 8 – Simulated cutting process of hair (a) 0.00ms (Start of skin compression), (b) 1.00ms (Skin bulge formed. Start of blade movement), (c) 1.14ms (Force on blade), (d) 1.22ms (Skin slipped along foil with reduction of friction due to deformation/retraction), (e) 1.26ms (Further deformation of skin resulted in increase of cutting force), (f) 1.40ms (Further separation of skin from foil led to force reduction. Blockage of hair provokes blade penetration into hair), (g) 1.44ms (Severance of hair), (h) 1.50ms (Re-bouncing of skin after cut), (i) 2.02ms (The skin is relaxed totally).

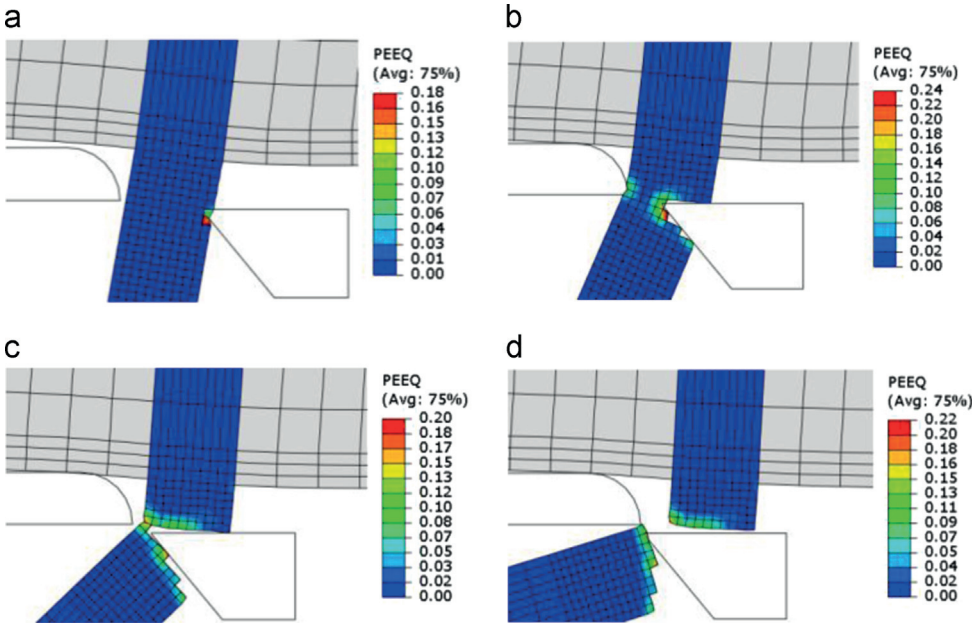

Fig. 10 – Simulation of hair damaging (Time instance t=1.40/1.50 correspond to plot "f/h" in Figs. 10 and 11.) a) t=1.40ms, b) t=1.46ms, c) t=1.48ms, d) t=1.50ms..

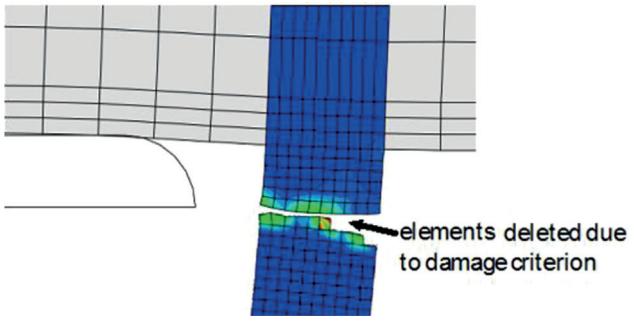

Fig. 11 – Time instance t=1.50 ms from Fig. 10 with severed hair end re-positioned to stubble to show impact of hair damage criterion.

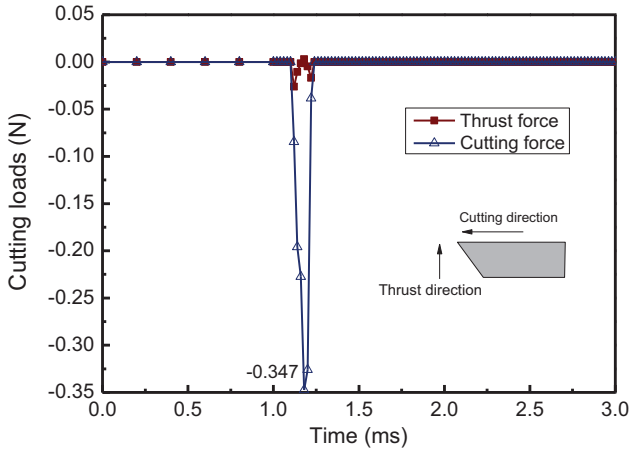

Fig. 12 – Cutting loads in case of skin with fixed boundary to the left.

shown. They demonstrate that the impact of this boundary condition on the magnitude of cutting forces is small. Contact conditions were defined for the interfaces: skin–foil, hair–blade and hair–foil. The friction coefficient of skin–foil was set to 0.16 (Bhushan et al., 2005), and to 0.4 (Wei and Bhushan, 2006) for hair–blade and hair–foil.

Objective of the simulation is to calculate the deformations and stress during the idealized dry shaving process. During this process, the skin is pressed against the foil so that the skin bulges into the foil aperture. Simultaneously, the cutting edge moves against the hair, captures it and cuts it. This simultaneous process is modeled via two distinct steps (Fig. 7).

The compression speed of foil to skin is 50 mm/s, and the compression amount is 50 μm. This magnitude was assumed corresponding to real shaving speeds and turned out to have little influence on calculation results. The cutting speed of blade is 900 mm/s. Considering the large deformation of skin, geometry nonlinearity (finite deformation) was included in the FEM model.

4. FEM simulation results and discussions

4.1. *Deformation of hair and skin*

Results of a simulation of the process of hair cutting are shown in Fig. 8.

Fig. 8a shows the initial state, Fig. 8b the status after step 1 (compression). The skin is compressed and bulges 10.9 μm into the aperture of the foil (Fig. 8b). The foil and blade moved towards the skin by 50 μm. From Fig. 8c–h, the cutting process is shown, where the blade moves towards the hair and cuts it. During this process, the skin deforms obviously. With the

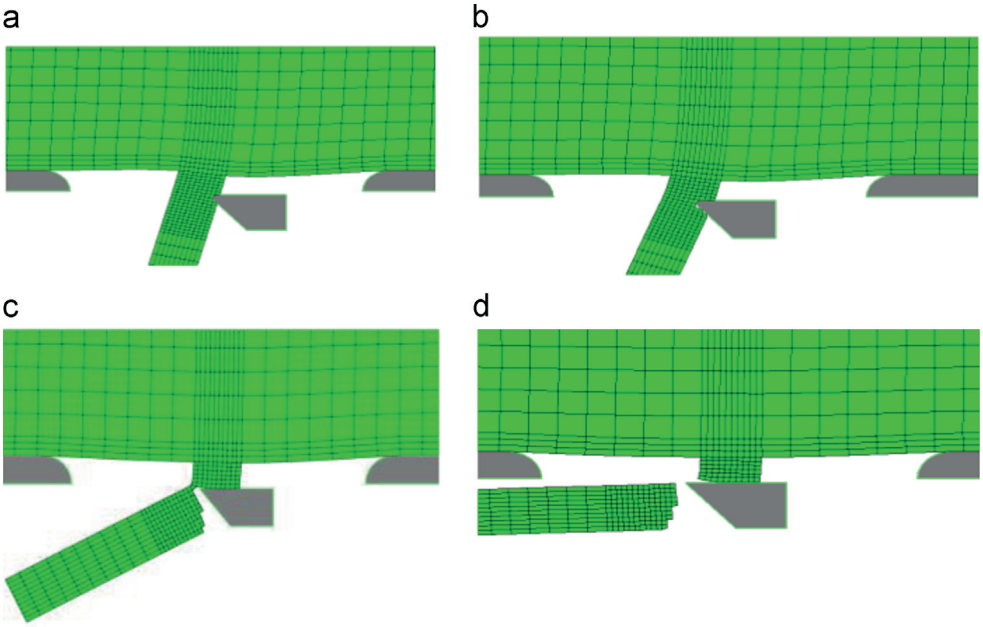

Fig. 13 – Deformation of hair and skin (a) t=1.18ms, (b) t=1.22ms, (c) t=1.24ms, (d) t=1.28ms.

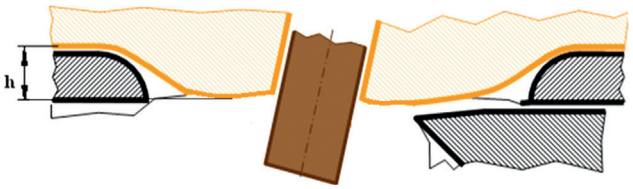

Fig. 14 – Schematics of skin bulge with definition of bulge height *h*.

Table 3 – Skin bulge height due to foil compression.

Foil compression depth (μm)	50	100	200
Formed skin bulge height *h* (μm)	10.93	22.61	49.39
Foil compression force (N)	0.20	0.46	0.92

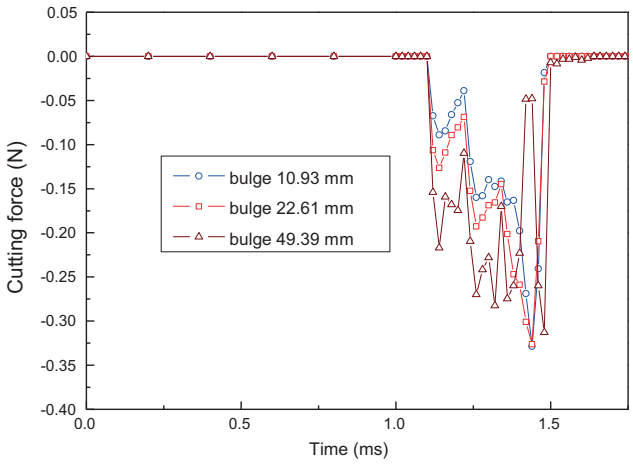

Fig. 15 – Cutting forces at different skin bulge heights.

blade stroke, the contact between skin and foil changes. Part of the skin looses contact to the foil. The main cause of this effect is the free boundary condition at the right and left sides of the skin. After the hair is cut off the skin bounces back (Fig. 8h). During bouncing back, the skin behaves like a pendulum with damping. It oscillates back and forth relative to the blade movement direction and attains equilibrium at approximately 2.02 ms (Fig. 8i).

4.2. *Cutting loads and damage process for unrestricted skin*

The calculated cutting loads onto the blade are shown in Fig. 9. The cutting force denotes the force component in the cutting direction and the thrust force means the component perpendicular to the cutting direction. The thickness of the plane model was selected to be 0.1 mm which is of the magnitude of the thickness of a hair. The simulations describe consequently the cutting of a hair with square cross-section with 0.1 mm width and negligible contact to the skin at two sides.

The letters within rectangles in Fig. 9 refer to the plots (a) to (h) in Fig. 8. While the blade pushes the hair to the foil edge, the cutting force grows rapidly. After the hair cutting, the force declines abruptly. At the beginning of contact between blade and hair, i.e. at somewhat before (c), the cutting force increases. At (c) equilibrium with friction between skin and foil upper surface is achieved, and the skin begins consequently to slip relative to the foil. The movement results in a deformation primarily of the hypodermis which is accompanied by a reduction of the pressure between skin and foil. The reduction of the contact pressure results in a reduction of friction; hence the cutting force declines between (c) and (d). From then up to instance (e) the skin is further deformed. The cutting force increases. Between (e) and (f) the left part of the skin separates further from the foil. Friction declines, the cutting force as well. With the separation of the left part, the contact pressure at the right is increasing. The friction

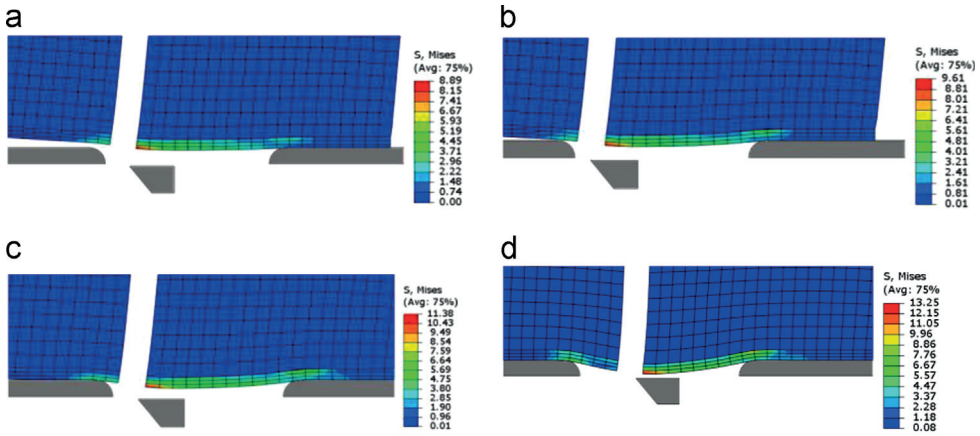

Fig. 16 – Stresses within skin as function of bulging depth. Maximum von Mises equivalent stress within epidermis (MPa) at the end of hair fracture), (a) bulge height =0.0μm, (b) bulge height =10.93μm, (c) bulge height =22.61μm, (d) bulge height =49.39μm

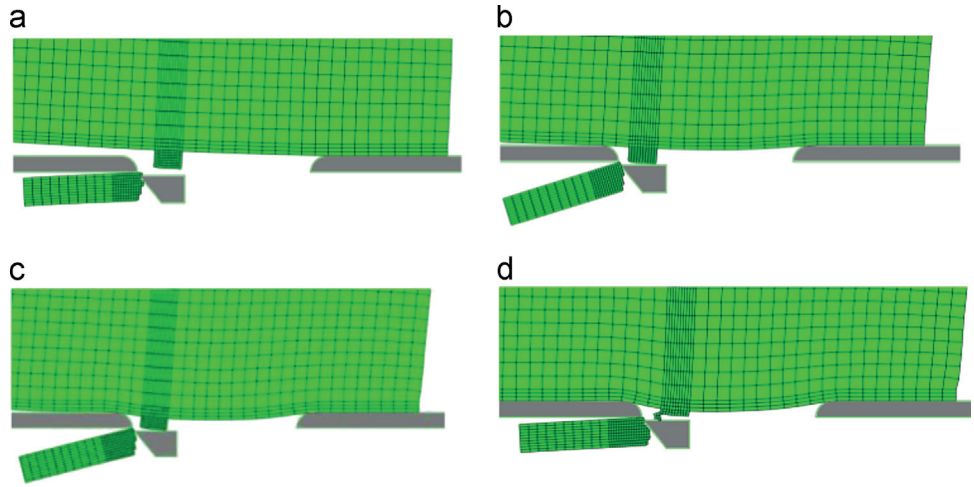

Fig. 17 – Hairs cut at different bulge heights, , (a) bulge height =0μm, (b) bulge height =10.93μm, (c) bulge height =22.61μm, (d) bulge height =49.39μm.

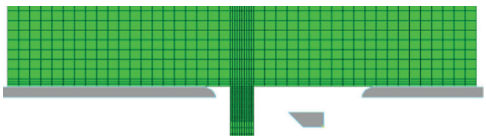

Fig. 18 – Hair initial position is close to the foil edge.

there begins to dominate at instance (f) resulting in a further increase of the cutting force. This instance coincides with the blade penetration into the hair. During cutting and fracture of hair, i.e. from (f) to (h) in Fig. 8, the force changes due to contact variation between hair and blade.

Calculated peak value of cutting force is 0.33 N, which is compatible with measurement values 0.18–0.31 N in the cutting experiment (Thozhur et al., 2007). It indicates that the FE models are reliable.

The damage process within the hair as predicted by the simulations is shown in detail in Fig. 10. The blade engages the hair at time 1.40 ms ((f) in Figs. 10 and 11) and moves the hair to the foil edge.

Contact between hair and foil edge is achieved at time 1.44 ms which coincides with the time instance (*g*) in Figs. 10 and 11 with maximum cutting force. Afterwards the cutting force declines so that skin and hair bounce back.

Damage was selected to be simulated corresponding to the shear damage initiation criterion of ABAQUS. The approach is well established in metal cutting. Whether it is justified in modeling of cutting hair must be justified by experiments. The consequences become apparent in Fig. 11. It repeats the time instance t=1.50 ms in Fig. 10 with the severed hair end re-positioned to the stubble. It shows the amount of deleted element. The deletion corresponds to an artificial crack opening and results in the prediction of smaller cutting forces. The present model has some limitations in fracture calculation due to the dependence on mesh size. Actual cracks of the hair should be smaller than the simulated results. A mesh will be 'deleted' when the criterial damage factor is reached. Thus, the crack is overstated inevitably because the hair cannot be discreted using coarser meshes than the actual crack scale, considering calculation efficiency.

Even the blade shape and cutting conditions in the present model are different from experiments (Thozhur et al., 2007). The

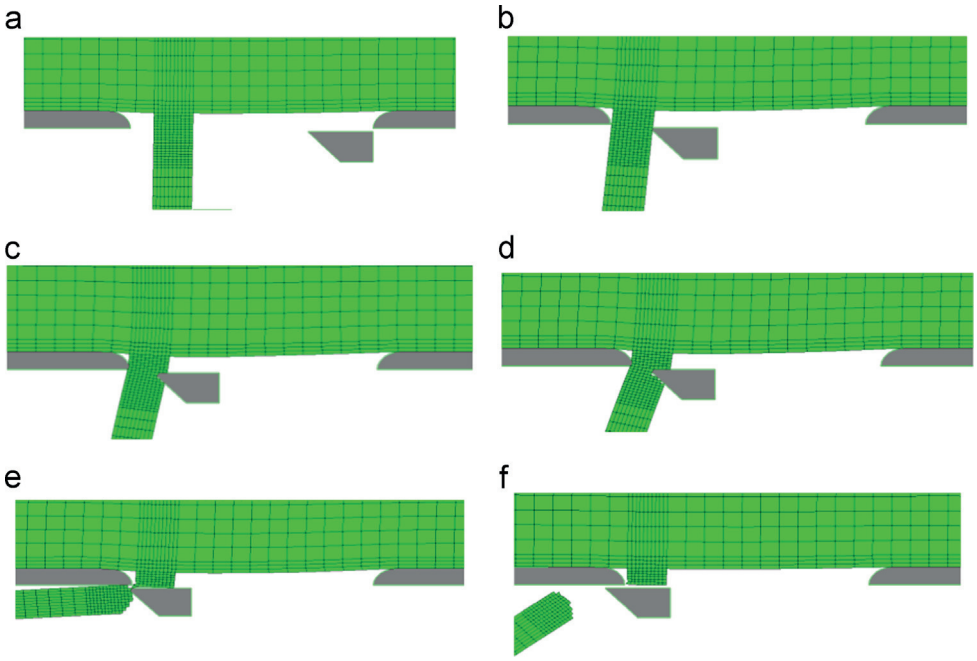

Fig. 19 – Hair cutting process for hair close to foil (Skin bulge height=10.93 μm, gap=10 μm). (a) 1.00 ms (skin compression finished), (b) 1.40 ms (blade penetrates into hair), (c) 1.44 ms (start of hair begun damaged), (d) 1.46 ms (damage in progress), (e) 1.52 ms (foil cuts the hair), (f) 1.56 ms (hair separated from main stem).

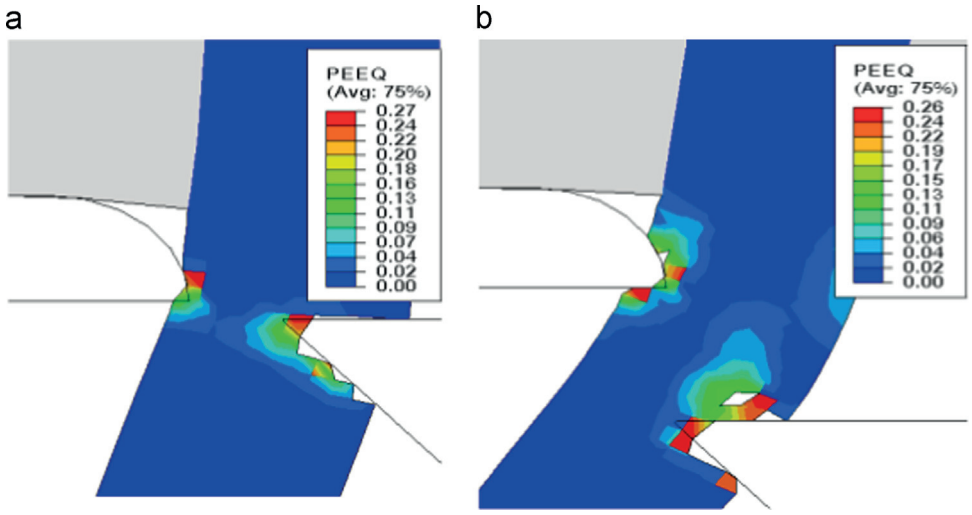

Fig. 20 – Plastic strain distribution within hair with stronger contribution of foil to cut, a) cutter-foil gap = 0.010mm, b) cutter-foil gap = 0.080mm.

"unclean" hair stubble all occurred in the experiment and simulation as shown Fig. 10. The fractured hair in the simulation results is consistent with the mechanism M2 (partial stable penetration followed by bending of hair and rapid fracture). This fracture mechanism M2 corresponds to the small clearance between blade and hair (less than the hair diameter).

4.3. *Effects of skin fixation at side boundaries*

The previous results were achieved under the assumption that the skin is free at the left and right boundaries. The other extreme condition avoids any deformation on the left boundary. The corresponding boundary condition fixes the left side of skin. Fig. 12 shows the corresponding cutting loads. It can be found that the fluctuations of cutting force during the increase (Fig. 9) disappeared (Fig. 12). The cutting force increases in the same way as between (b) and (c) in Fig. 9. With respect to the thrust force of blade, the force fluctuations are almost eliminated.

It indicates that in case of fixed skin boundaries the cutting time is much smaller than in case of free boundaries as shown in Fig. 9. Deformation and damage results are shown in Fig. 13. The fixed skin boundary contributes to the hair's damage earlier than that with free skin boundary. The hair is not moved to the foil edge which is typically seen in reality. The fixed boundary results thus in a too stiff skin and is consequently not applied during the following simulations.

4.4. Effects of skin bulge height on cutting results

Before the blade movement and before hair cutting, the foil compresses the skin and the skin forms a bulge (Fig. 14). Due to the elastic properties of skin, there is a difference between the compression depth of foil and skin bulge height. The skin bulge height is less than the depth of skin compression. Simulation results are summarized in Table 3. The cutting forces at different skin bulges are shown in Fig. 15.

The forces increase to peak values near the end of the cutting processes which are almost independent of the bulging depth. An impact of bulging can be observed during the initial phase. Cutting forces increase stronger in case of higher skin bulges. This phenomenon can be explained with the larger compression force in case of larger bulge heights. The higher compression force leads to a larger friction force between skin and foil which supports the hair when moved to the foil edge during hair cutting.

Stress within the skin as function of bulge height is shown in Fig. 16. When the skin forms a higher bulge, the skin will experience larger stress. Fractured hairs and stubbles formed at different skin bulges are shown in Fig. 17. The residual stubble length decreases with the increasing skin bulge.

4.5. Contribution of foil edge to cutting

For typical dry shaving conditions, hair is cut simultaneously by the blade and the foil edge. They are like a pair of scissors. Their efficacy depends on the clearance between them.

In the simulation results listed in Figs. 16 and 17, the severance of hair is achieved by the blade edge. The foil edge forms in cases of smaller bulging an anvil as follows from Fig. 16a and b or has no contact before hair separation as in Fig. 16c and d in cases of deeper bulging. One cause of this phenomenon is that the initial distance between hair and foil edge is too long. Another reason may be that the selected skin model may be effectively too stiff as a consequence of the fixation of the inner layer of the hypodermis.

In the geometry models above the hair is initially anticipated within the center of the foil aperture. Actually, it may be found at any position within apertures and thus also closer to the foil edge as within the model in Fig. 18.

The simulation results for the cutting process of hair are shown in Figs. 19 and 20. Before the blade is moved, the skin was compressed by 50 μm. Because the initial position of hair was close to the foil, the foil blocked the hair movement and penetrated into the hair. At areas in contact with the foil edge, deformation concentration occurred (Fig. 20). However, the foil edge is more like a block rather than a cutter during cutting. Compared with the blade, the foil edge cuts only a little part of hair.

4.6. Effects of clearance between foil edge and blade on cutting results

To investigate the effect of clearance between the blade and the foil edge on cutting results, simulations for the five values

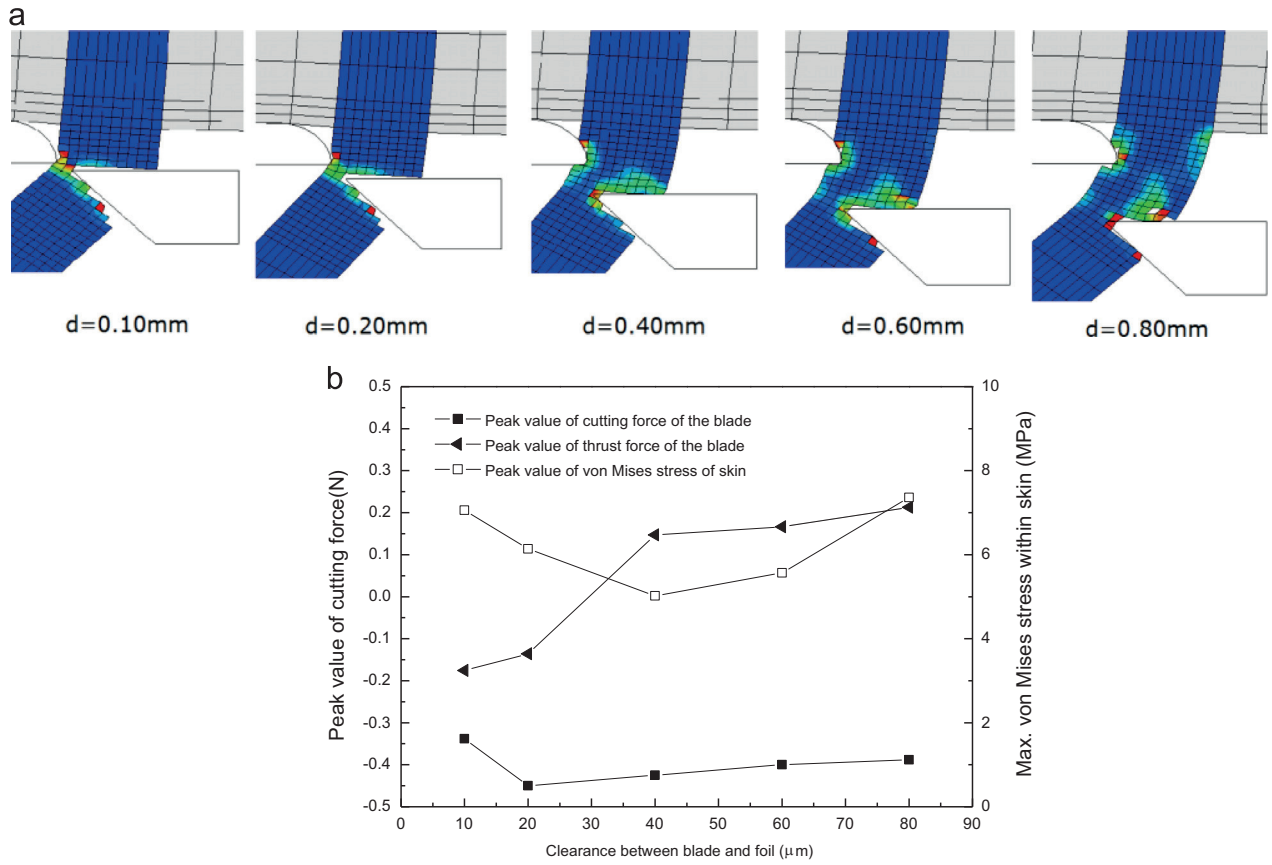

Fig. 21 – Cutting at varying clearance between blade and foil (skin compression 0.05 mm) (a) deformation and damage of hairs; (b) maximal von Mises stress within skin, cutting force and thrust force of the blade.

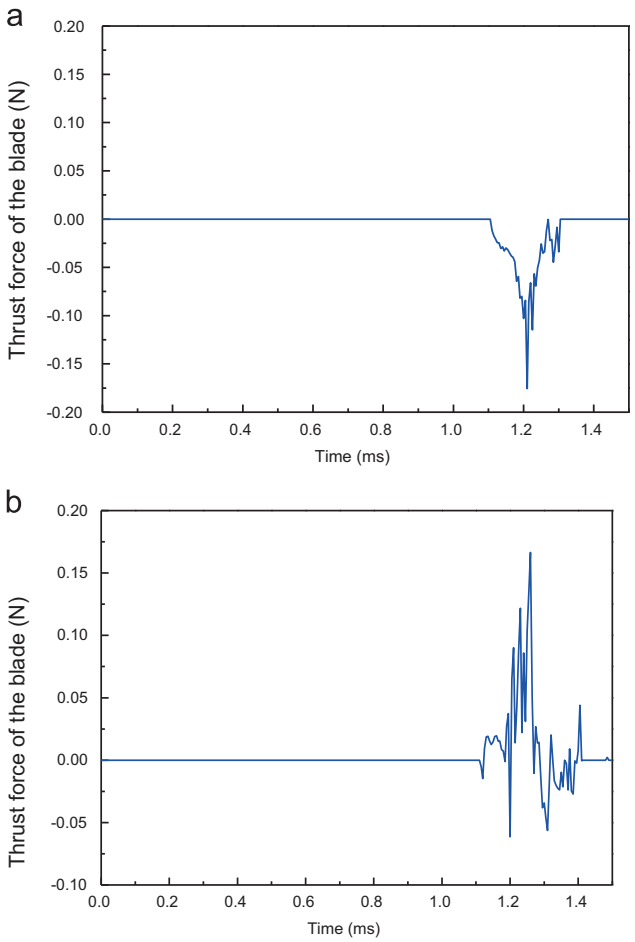

Fig. 22 – The thrust forces of the blade at the clearance (a) 10 μm and (b) 60 μm.

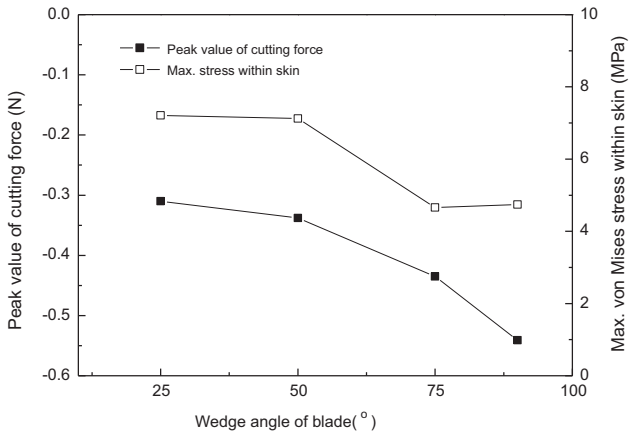

Fig. 23 – Max von Mises stress within skin and cutting force varying with wedge angle of blade (blade thickness is 100 μm).

of clearance of 10, 20, 40, 60 and 80 μm were performed. Results of cutting forces and skin stress are summarized in Fig. 21. With respect to skin stress, the varying with the clearance is saddle-like.

For the clearance 40 μm, the skin stress is lowest. The influence of the clearance on cutting force is little. When the blade has sharper wedge angle than the foil, the foil is like a block rather than a cutter. So the cutting force at different clearance varies little. The large clearance cannot lead to the low cutting force but leave the longer stubble and the higher skin stress. So the clearance between the blade and the foil has to be maintained within a limited distance. Due to the support from the soft skin and hair damage, the thrust force of the blade has severe fluctuations with the cutting process. When the clearance is small, the thrust is in only one direction (Fig. 22a). But, the thrust force of the blade fluctuates up and down (Fig. 22b). Even though, the peak value of thrust force of the blade has little variation with the clearance.

4.7. *Effects of blade geometry on cutting results*

With the same thickness of blade, i.e. with 100 μm, simulations with the four values of wedge angle: 25°, 50°, 75° and 90° for blade were conducted. The simulations of hair cutting were carried out with the four blades. Other conditions were maintained unchanged. The cutting forces of blade and skin stresses calculated by the FEM simulation are listed in Fig. 22. The cutting force grows with the increasing wedge angle of the blade. Because the larger wedge angle means that the blade is blunter, the hair cutting with such blades needs the larger forces. The cutting force is 0.33 N for the sharp blade (wedge angle 25°), and increases to 0.54 N for the blunt blade (wedge angle 90°). At the same time, it can be found that the stress in skin decreases with the wedge angle of the blade. When the wedge angle of the blade grows, the contribution of the foil to hair cutting is larger, and the pull force of the blade to the skin is low (Fig. 23). On the contrary, the sharp blade with the small wedge angle cuts the hair without the action of the foil, and the skin is pulled by the blade. It can be found from Fig. 24 that the skin has higher stress in the case of the blade with smaller wedge angle.

When the blade is blunt (wedge angle is large), the foil plays a more active role in cutting than in the case with a sharper blade. Fig. 25 shows the resulting hair stubble and the

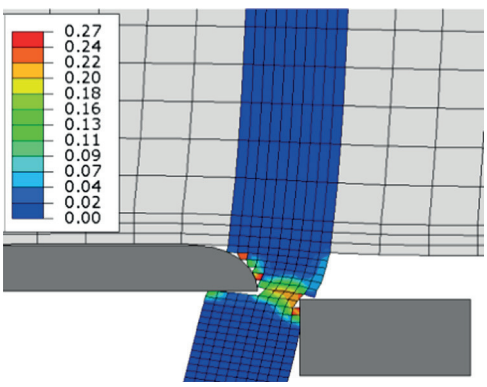

Fig. 24 – Equivalent plastic strain distributed in hair with a blunt blade (the blade wedge angle is 90°, and thickness is 100 μm).

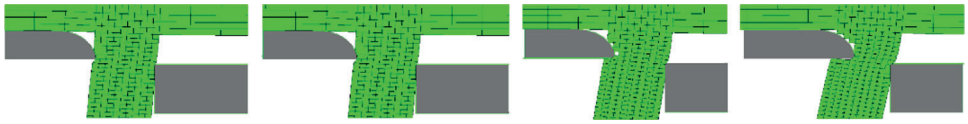

Fig. 25 – The hair severance under the action of blade and foil ((the blade wedge angle is 90°, and thickness is 100 μm).

fractured hair end. Almost half of the hair is damaged by the foil.

5. Conclusions

For the numerical simulation of hair (beard) cutting, 2-D FEM models of dry shaving were built within ABAQUS. The fracture of hair during cutting was captured by the shear damage initiation criterion of ABAQUS. The results show the typical phenomena in beard cutting: skin bulges into the foil apertures, hairs are moved together with the surrounding skin to the adjacent aperture rims, are cut there and bounce back into their initial locations. Cutting is primarily achieved by the undercutter/blade. The aperture rims form anvils. There is a contribution of the aperture rims to cutting, it is comparatively small and increases with decreasing edge angle. The length of the residual hair stubbles depend on the depth the skin bulges into the apertures.

Influences of the skin bulge, clearance between blade and foil and blade geometry on cutting results are analyzed, some conclusions can be drawn out as

1) The skin bulge formed in the foil aperture by the compression before cutting increases almost linearly with compression force. The cutting forces increase to peak values near the end of the cutting processes which are almost independent of the bulging depth. An impact of bulging can be observed during the initial phase. Cutting forces increase stronger in case of higher skin bulges. This phenomenon can be explained with the larger compression force in case of larger bulge heights. The higher compression force leads to a larger friction force between skin and foil which supports the hair when moved to the foil edge during hair cutting.
2) When the skin forms a higher bulge, it will also experience larger stress. The length of residual stubbles decreases with increasing skin bulge. There is less contact between skin and foil during hair cutting at smaller skin bulges which leads to longer cutting times.
3) With the increasing clearance between blade and foil, the peak value of cutting force has little change and the maximum skin stress has saddle-like change. At the clearance 0.04 mm, the skin stress has the lowest value impact on thrust component. The thrust force of the blade fluctuates with the cutting process, and the larger clearance leads to severe fluctuations up and down.
4) Large wedge angles lead to high peak values of cutting forces. The influence of wedge angle on skin stress is not obvious, for it is influenced by the foil shape, skin bulge and friction conditions. The role of the foil edge in beard cutting is influenced by the wedge angle of the blade. When the sharp blade is used (with the smaller wedge angle), the hair is cut quickly without contact with the foil. On the contrary, the foil has to cut the hair cutting when the blunt blade is used, where the scissor is formed.

Acknowledgement

Thanks are due to Dr. Jian-Han Zhang for giving useful suggestions of numerical models of hair cutting.

REFERENCES

Barnes, H.A., Roberts, G.P., 2000. The non-linear viscoelastic behaviour of human hair at moderate extensions. Int. J. Cosmet. Sci. 22, 259–264.
Bhushan, B., Wei, G., Haddad, P., 2005. Friction and wear studies of human hair and skin. Wear 259, 1012–1021.
Bhushan, B., 2008. Nanoscale characterization of human hair and hair conditioners. Process. Mater. Sci. 53, 585–710.
Dawber, R., 1996. Hair: its structure and response to cosmetic preparations. Clin. Dermatol. 14, 105–112.
Delalleau, A., Josse, G., Lagarde, J.-M., Zahouani, H., Bergheay, J.-M., 2008. A nonlinear elastic behavior to identify the mechanical parameters of human skin in vivo. Skin Res. Technol. 14, 152–164.
Draelos, Z.D., 2012. Male skin and ingredients relevant to male skin care. Br. J. Dermatol. 166 (s1), 13–16.
Flynn, C., McCormack, B.A.O., 2008. Finite element modeling of forearm skin wrinkling. Skin Res. Technol. 14, 261–269.
Gillette K.C., A safety razor shaver with disposable blades, US Patent 775134, 1904.
Pailler-Mattei, C., Beca, S., Zahouani, H., 2008. In vivo measurements of the elastic mechanical properties of human skin by indentation tests. Med. Eng. Phys. 30, 599–606.
Pellacani, G., Seidenariv, S., 1999. Variations in facial skin thickness and echogenicity with site and age. Acta Derm. Venereol. 79, 366–369.
Sakon, S., Hamada, T., Fujimoto, S., Umesaki, N., Kobayashi, A., 2009. Surface modification of electric hair clipper blade for increasing its lifetime. Vacuum 83, 119–123.
Seshadri, I.P., Bhushan, B., 2008. In situ tensile deformation characterization of human hair with atomic force microscopy. Acta Mater. 56, 774–781.
Thozhur, S.M., Crocombe, A.D., Smith, P.A., Cowley, K., Mullier, M., 2007. Cutting characteristics of beard hair. J. Mater. Sci. 42, 8725–8737.
Thozhur, S.M., Crocombe, A.D., Smith, P.A., Cowley, K., Mullier, N., 2006. Structural characteristics and mechanical behaviour of beard hair. J. Mater. Sci. 41, 1109–1121.
van de Sompela, D., Kongb, T.Y., Ventikosa, Y., 2009. Modeling of experimentally created partial-thickness human skin burns

and subsequent therapeutic cooling: a new measure for cooling effectiveness. Med. Eng. Phys. 31, 624–631.
Wei, G., Bhushan, B., 2006. Nanotribological and nanomechanical characterization of human hair using a nanoscratch technique. Ultramicroscopy 106, 742–754.
Wiltton, J.T., Everal, J.D., 1973. The thickness of epidermis. Br. J. Dermatol. 89 (5), 467–476.
Wu, J.Z., Cutlip, R.G., Welcome, D., Dong, R.G., 2006. Estimation of the viscous properties of skin and subcutaneous tissue in uniaxial stress relaxation tests. Bio-Med. Mater. Eng. 16, 53–66.
Xu, B., Chen, X., 2011. The role of mechanical stress on the formation of a curly pattern of human hair. J. Mech. Behav. Biomed. Mater. 4, 212–221.